Supporting Information for

Interfacial acidity on the strontium titanate surface: A scaling paradigm and the role of the hydrogen bond

Robert C. Chapleski, Jr.,[†] Azhad U. Chowdhury,[§] K. Reid Mason,[†] Robert L. Sacci,[§] Benjamin Doughty,[*,§] and Sharani Roy[*,†]

† Department of Chemistry, University of Tennessee, Knoxville, TN 37996, USA
§ Chemical Sciences Division, Oak Ridge National Laboratory, Oak Ridge, TN 37831, USA

Table of Contents

I. Computational Results

I.A. Surface stability of TiO_2-terminated STO(100) versus SrO-terminated STO(100)

Two different (100) faces can be prepared from a crystalline sample of STO: one which presents a TiO_2 surface, and the other which presents an SrO surface. To determine the relative stability of these two surface terminations, two supercells of STO(100) were constructed, each consisting of a 3 × 3 × 3 slab with an adlayer of surface atoms in order to present the same surface termination to the vacuum on both sides of the slab. The first slab contained 162 atoms, which exposed two TiO_2 surfaces to the vacuum, and the other contained 153 atoms, which exposed two SrO surfaces to the vacuum, as shown in Figure S1. Using the DFT geometry-optimization scheme described in the Methods section of the main text, wherein the top surface layer (45 atoms for each slab) was allowed to relax, the TiO_2-terminated slab (surface energy = 0.093 eV/Å^2) was found to present a more stable surface than the SrO-terminated slab (surface energy = 0.098 eV/Å^2). Surface energies were calculated using the following equation:

$$E_{surf} = \frac{1}{A}[E_{slab} - nE_{bulk}],$$

where E_{surf} is the surface energy of the slab, A is the total surface area of the slab (including both surfaces presented to the vacuum), E_{slab} is the electronic energy of the slab, n is the number of atoms in the slab, and E_{bulk} is the electronic energy per atom of bulk STO.[1]

A preliminary set of adsorption calculations revealed that isopropanol adsorbs more strongly on TiO_2-terminated STO(100) than on SrO-terminated STO(100) by 0.49 eV. Details are provided in Figure S2. Due to greater surface stability in vacuum as well as stronger isopropanol adsorption, the TiO_2-terminated surface was selected for our computational study of alkanol adsorption on STO(100).

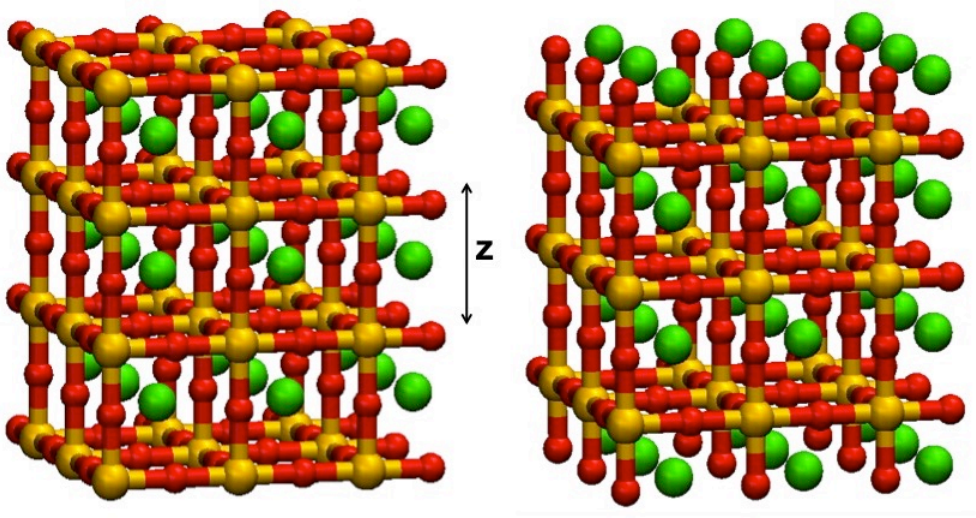

Figure S1: TiO_2- (left) and SrO-terminated (right) slabs of STO(100). Same color scheme as in Figure 1 of the main text.

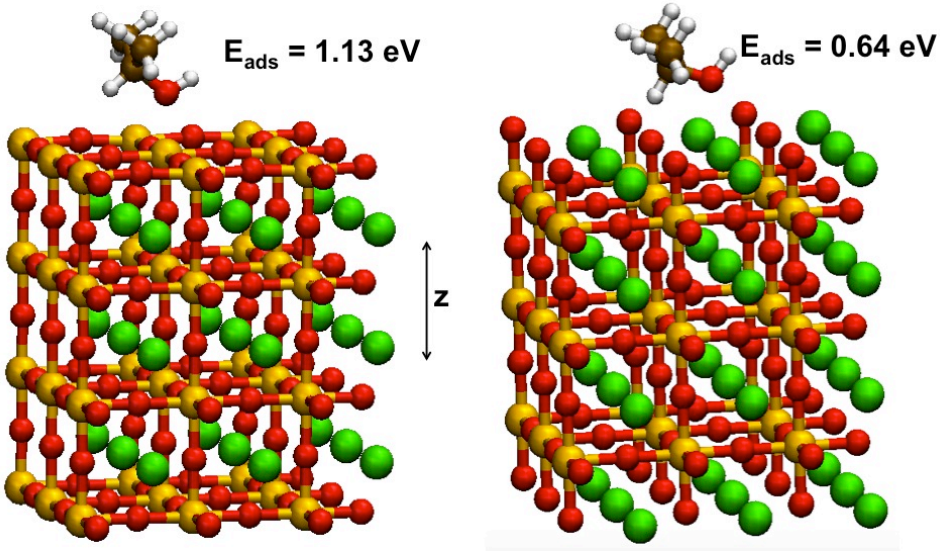

Figure S2: Adsorption of isopropanol on TiO_2- (left) and SrO-terminated (right) slabs of STO(100). Here, a lattice constant of 4.00 Å and a U value of 11.3 eV for Ti 3d orbitals were used. Same color scheme as in Figure 1 of the main text.

I.B. Site of isopropanol adsorption on TiO_2-terminated STO(100)

Several adsorption sites for isopropanol adsorption on the TiO_2-terminated surface of STO(100) were considered by incrementally translating isopropanol across the surface and adsorbing it at different sites. To initiate this two-dimensional potential-energy-surface (PES) scan, isopropanol was placed above the surface, with the α-carbon atom

directly above a subsurface Sr atom (represented in Figure S3), both methyl groups positioned away from the surface, and the -OH group positioned toward the surface. This geometry was then partially optimized, freezing the entire STO slab as well as the x- and y- coordinates of the α-carbon atom (i.e., those dimensions parallel to the surface) in order to fix the molecule above the Sr atom. The energy of the structure resulting from optimization of the remaining isopropanol atomic coordinates was then recorded. This partial optimization procedure was repeated at incremental points along the STO(100) surface, at points marked with "+" in Figure S3. All resulting structures are presented in Figure S4, superposing a contour plot of corresponding isopropanol adsorption energies. We find that the strongest adsorption occurs when the isopropanol O atom is oriented above a Ti atom. We note that, in this scan, Grimme's D3 dispersion correction was not included, and thus, adsorption is markedly weaker than that reported in the main text. The most favorable adsorption site is circled in Figure S4, and this result was used as the starting geometry for the "α-H close" optimization described in the Methods section of the main text.

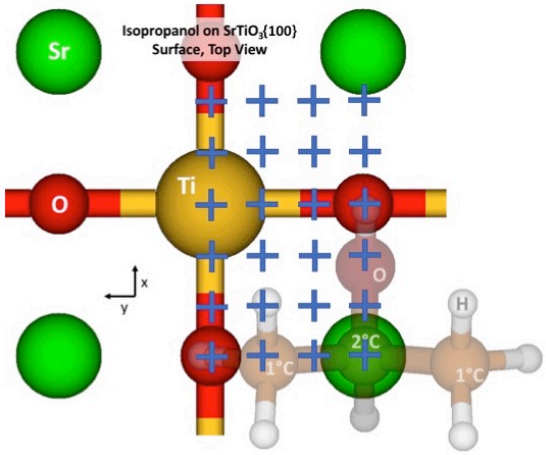

Figure S3: A schematic showing the placement of isopropanol, marked by "+", over the TiO_2-terminated surface of STO(100) in a partially-optimized two-dimensional PES scan.

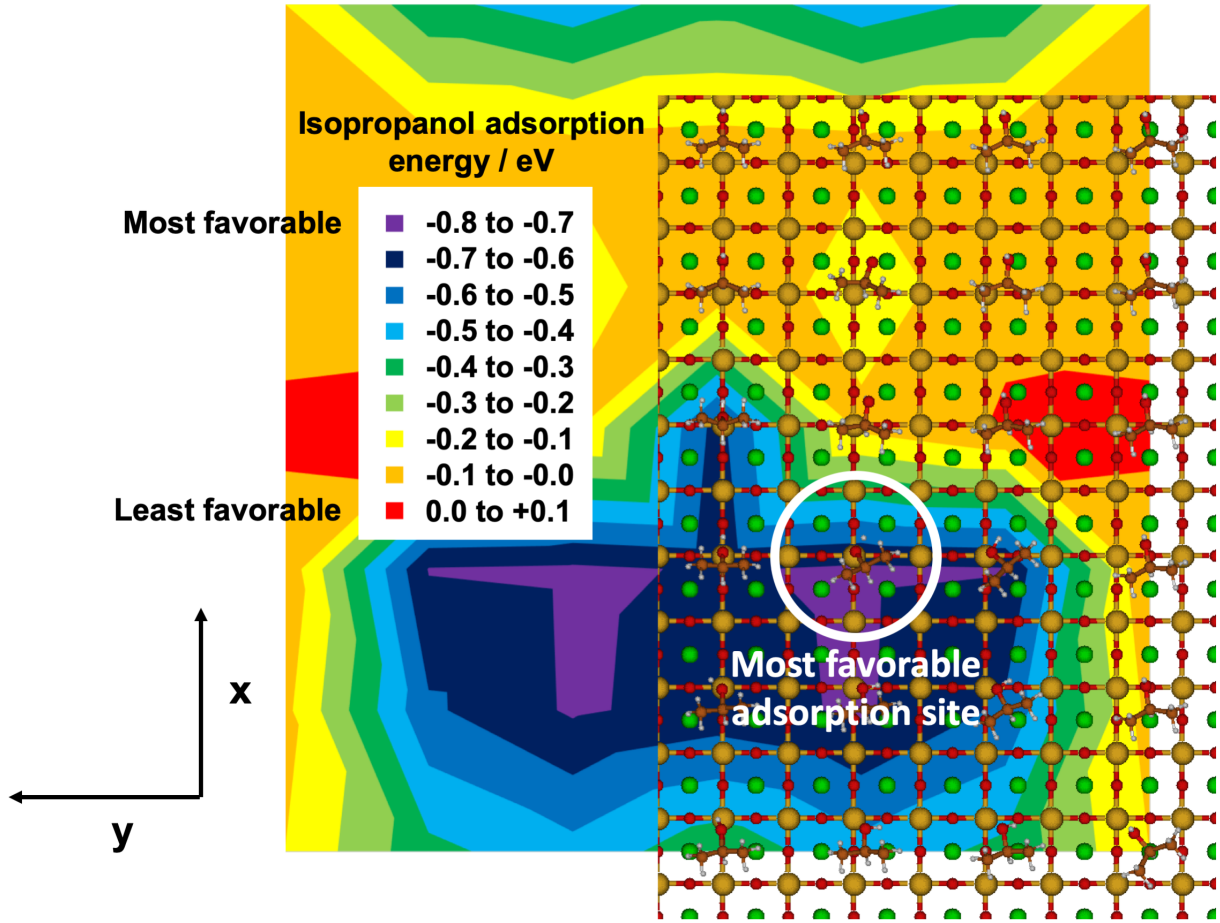

Figure S4: Contour plot showing isopropanol adsorption energies on STO(100) for all structures resulting from the two-dimensional PES described in Figure S3.

I.C. Selected structural data for isopropanol adsorbed on STO(100)

Figure S5 shows a close-up structure of deprotonated, hydrogen-bonded isopropanol adsorbed on STO(100) in the "α-H close" orientation. Identified in the figure are several interatomic distances (left panel) and angles (right panel) that are presented in Tables S1-S3 for the three orientations of adsorbed isopropanol shown in Figure 2 of the main text. In Figure S5, the Ti atom indicated is that which interacts with O_{alk} during adsorption, and the H_{hyd}-O_{surf}-(0,0,1) angle refers to that between the H_{hyd}-O_{surf} bond and the surface normal. The subscript, "surf" denotes the surface and the subscript, "alk" denotes the alkoxy moiety.

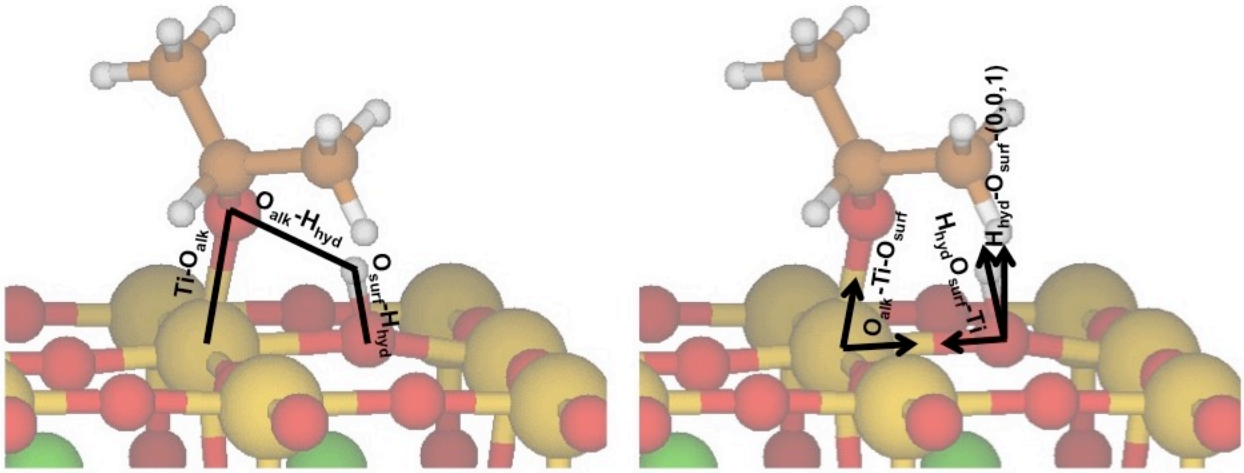

Figure S5: Close-up optimized structure of deprotonated, hydrogen-bonded isopropanol in the "α-H close" orientation, on STO(100), with several structural features indicated.

Table S1: Selected interatomic distances and angles for optimized structures of "α-H close," as shown in Figures 1 and 2 of the main text

"α-H close"	Molecular, physisorbed	Deprotonated, Hydrogen-bonded	Deprotonated, broken-hydrogen-bonded
$Ti\text{-}O_{alk}$	2.20 Å	1.96 Å	1.91 Å
$O_{alk}\text{-}H_{hyd}$	0.98 Å	1.90 Å	2.78 Å
$O_{surf}\text{-}H_{hyd}$	2.38 Å	0.99 Å	0.98 Å
$O_{alk}\text{-}Ti\text{-}O_{surf}$	83.1°	77.9°	87.3°
$H_{hyd}\text{-}O_{surf}\text{-}(0,0,1)$	89.8°	14.7°	64.0°
$H_{hyd}\text{-}O_{surf}\text{-}Ti$	97.3°	81.1°	94.6°

Table S2: Selected interatomic distances and angles for optimized structures of "CH_3 away," as shown in Figures 1 and 2 of the main text.

"CH_3-away"	Molecular, physisorbed	Deprotonated, hydrogen-bonded	Deprotonated, broken-hydrogen-bonded
$Ti\text{-}O_{alk}$	2.20 Å	1.95 Å	1.92 Å
$O_{alk}\text{-}H_{hyd}$	0.98 Å	1.85 Å	2.81 Å
$O_{surf}\text{-}H_{hyd}$	2.72 Å	1.00 Å	0.98 Å
$O_{alk}\text{-}Ti\text{-}O_{surf}$	86.1°	76.4°	87.8°
$H_{hyd}\text{-}O_{surf}\text{-}(0,0,1)$	83.2°	13.9°	65.6°
$H_{hyd}\text{-}O_{surf}\text{-}Ti$	103.3°	81.2°	95.2°

Table S3: Selected interatomic distances and angles for optimized structures of "α-H away," as shown in Figures 1 and 2 of the main text.

"α-H away"	Molecular, physisorbed	Deprotonated, hydrogen-bonded	Deprotonated, broken-hydrogen-bonded
$Ti\text{-}O_{alk}$	2.22 Å	1.95 Å	1.91 Å
$O_{alk}\text{-}H_{hyd}$	0.98 Å	1.93 Å	2.83 Å
$O_{surf}\text{-}H_{hyd}$	2.23 Å	0.99 Å	0.98 Å
$O_{alk}\text{-}Ti\text{-}O_{surf}$	79.1°	77.9°	88.2°
$H_{hyd}\text{-}O_{surf}\text{-}(0,0,1)$	94.7°	16.6°	65.7°
$H_{hyd}\text{-}O_{surf}\text{-}Ti$	95.4°	82.5°	94.7°

I.D. Energy pathways for chemisorption and proton transfer

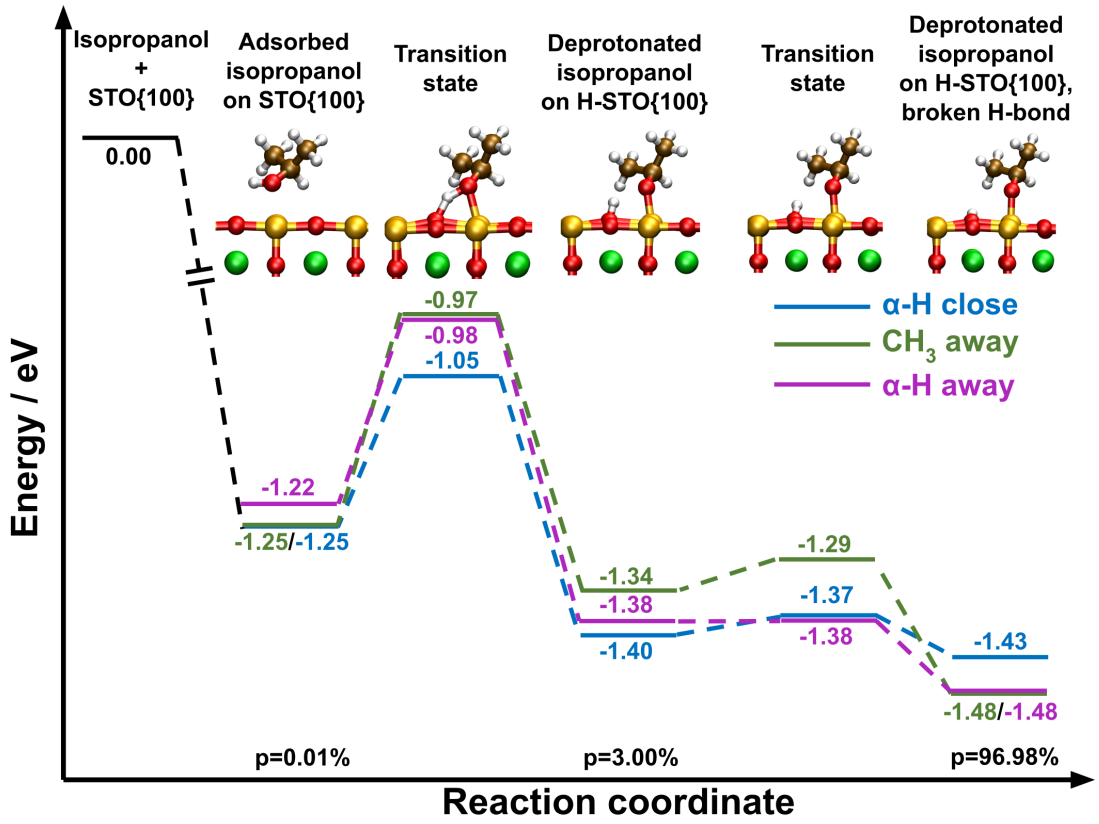

Figure S6: Energy pathway of adsorption and proton transfer of isopropanol on STO(100) calculated using DFT for all molecular orientations shown in Figs. 1 and 2 of the main text. *p* values are sums of Boltzmann populations of all orientations for a given species at 298 K. Insets show geometries of stationary points along the "α-H close" pathway. Same color scheme as in Fig. 1 of the main text.

To test the sensitivity of our qualitative results to the choice of functional and the choice of dispersion correction, we compared the adsorption energies and activation energies calculated using the PBE+D3 method described in the main text to corresponding energies using (a) the PBE+D3BJ method, i.e., the PBE functional implemented with Grimme's D3 dispersion correction and Becke-Johnson (BJ) damping, and (b) the RPBE+D3 method, i.e., the RPBE functional implemented with Grimme's D3 dispersion correction. The energies were calculated by performing single-point calculations using the PBE+D3BJ and RPBE+D3 methods on geometries optimized using the original PBE+D3 method.

Tables S4, S5, and S6 show that the species along the energy pathways for the different orientations of isopropanol are stabilized upon changing the functional from PBE to RPBE, but the energy differences between species within a pathway are similar between PBE and RPBE, implying that the qualitative results do not change from PBE to RPBE. Further, our comparison shows that the changes in results due to the addition of Becke-Johnson damping to the dispersion correction are minimal.

Table S4: Energies of the species along the energy pathway for the "α-H close" orientation of isopropanol on STO(100), calculated using PBE+D3, PBE+D3BJ, and RPBE+D3 functionals. The species are presented in the order shown in Fig. S6.

Method	Adsorbed isopropanol (eV)	Transition state (eV)	Deprotonated isopropanol (H-bonded) (eV)	Transition state (eV)	Deprotonated isopropanol (H-bond broken) (eV)
PBE+D3	-1.25	-1.05	-1.40	-1.37	-1.43
PBE+D3BJ	-1.24	-1.05	-1.39	-1.35	-1.42
RPBE+D3	-1.49	-1.23	-1.61	-1.66	-1.70

Table S5: Energies of the species along the energy pathway for the "CH_3 away" orientation of isopropanol on STO(100), calculated using PBE+D3, PBE+D3BJ, and RPBE+D3 functionals. The species are presented in the order shown in Fig. S6.

Method	Adsorbed isopropanol (eV)	Transition state (eV)	Deprotonated isopropanol (H-bonded) (eV)	Transition state (eV)	Deprotonated isopropanol (H-bond broken) (eV)
PBE+D3	-1.25	-0.97	-1.34	-1.29	-1.48
PBE+D3BJ	-1.24	-0.97	-1.34	-1.29	-1.47
RPBE+D3	-1.49	-1.13	-1.53	-1.52	-1.75

Table S6: Energies of the species along the energy pathway for the "α-H away" orientation of isopropanol on STO(100), calculated using PBE+D3, PBE+D3BJ, and RPBE+D3 functionals. The species are presented in the order shown in Fig. S6.

Method	Adsorbed isopropanol (eV)	Transition state (eV)	Deprotonated isopropanol (H-bonded) (eV)	Transition state (eV)	Deprotonated isopropanol (H-bond broken) (eV)
PBE+D3	-1.22	-0.98	-1.38	-1.38	-1.48
PBE+D3BJ	-1.21	-0.97	-1.38	-1.37	-1.46
RPBE+D3	-1.46	-1.14	-1.59	-1.62	-1.73

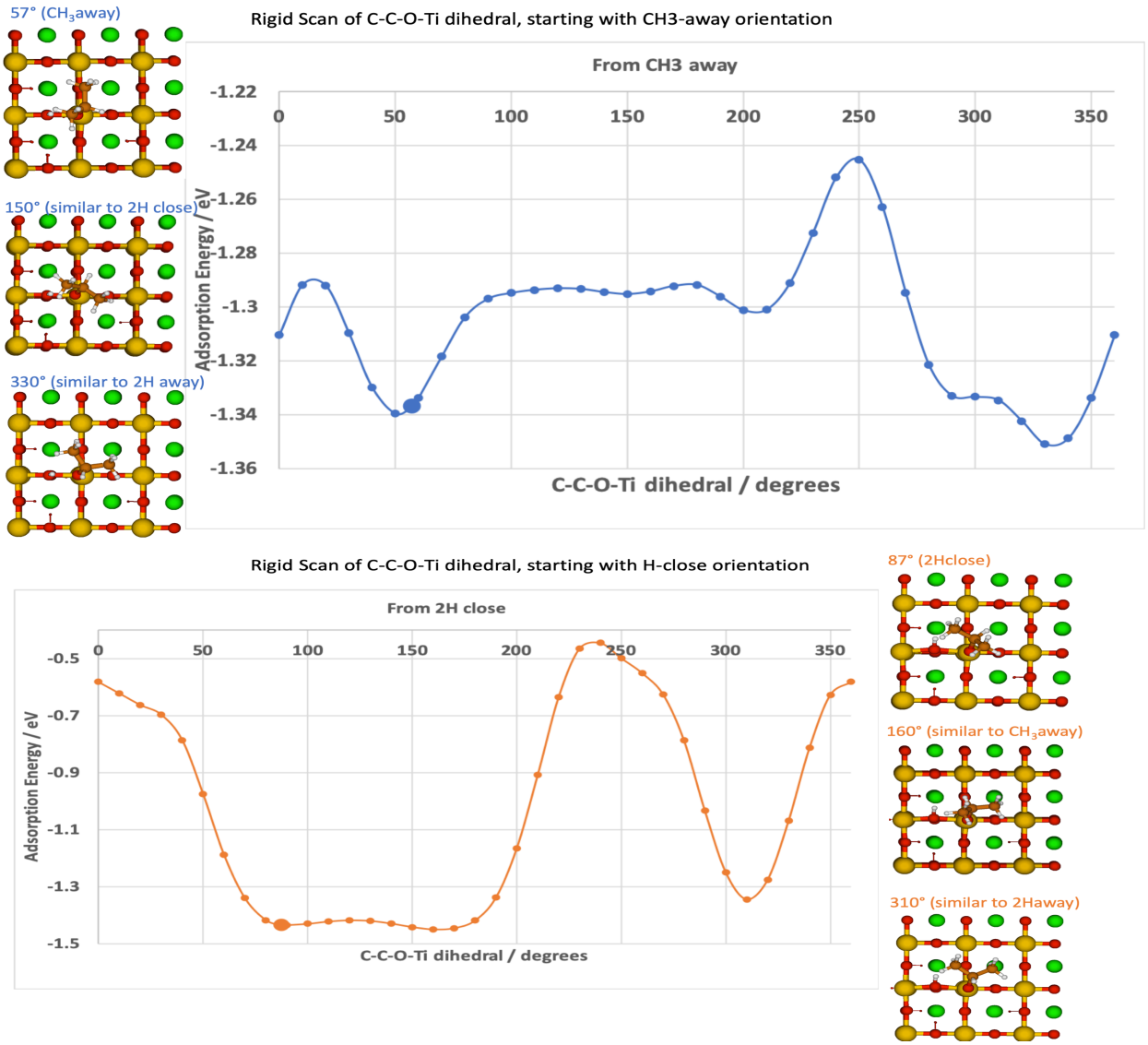

Figure S7: Rotational energy scan of the chemisorbed, deprotonated isopropanol on STO(100). The top panel shows the H-bonded species and the bottom panel shows the H-bond broken species. The molecule was rotated by 360° about the C-C-O-Ti dihedral angle, keeping the rest of the molecule and the surface atoms fixed. "2H" corresponds to "α-H", denoting that the hydrogen is bound to a secondary carbon.

I.E. Vibrational frequencies and hydrogen-bonding strength

Table S7 provides O_{surf}-H_{hyd} stretching and wagging frequencies for four alkanols. A reverse trend is revealed for wagging frequencies when compared to those of stretching, in line with our expectations regarding hydrogen-bond strength.

Table S7: DFT-computed O_{surf}-H_{hyd} stretching and wagging frequencies (cm^{-1}) of selected chemisorbed, hydrogen-bonded alkanols in the "α-H close" orientation.

	O_{surf}-H_{hyd} stretch	O_{surf}-H_{hyd} wag
Methanol	3383	1027
Ethanol	3331	1030
Isopropanol	3359	1023
Sec-butanol	3440	1021

Table S8: DFT O-H stretching vibrational frequencies (cm^{-1}) of the adsorbed isopropanol species shown in Figures 1 and 2 of the main text. The last column gives the mean of the three frequencies, along with the average of the absolute values of the deviation of each frequency from the mean.

	"α-H close"	"CH_3 away"	"α-H away"	Average ± Avg. |Deviation|
Physisorbed (protonated) - O_{alk}-H_{hyd} stretch	3617	3647	3579	3614 ± 23
Deprotonated, hydrogen-bonded O_{surf}-H_{hyd} stretch	3359	3325	3405	3363 ± 28
Deprotonated, broken-hydrogen-bonded O_{surf}-H_{hyd} stretch	3581	3579	3582	3581 ± 1

I.F. Selected data for alkanols adsorbed on STO(100)

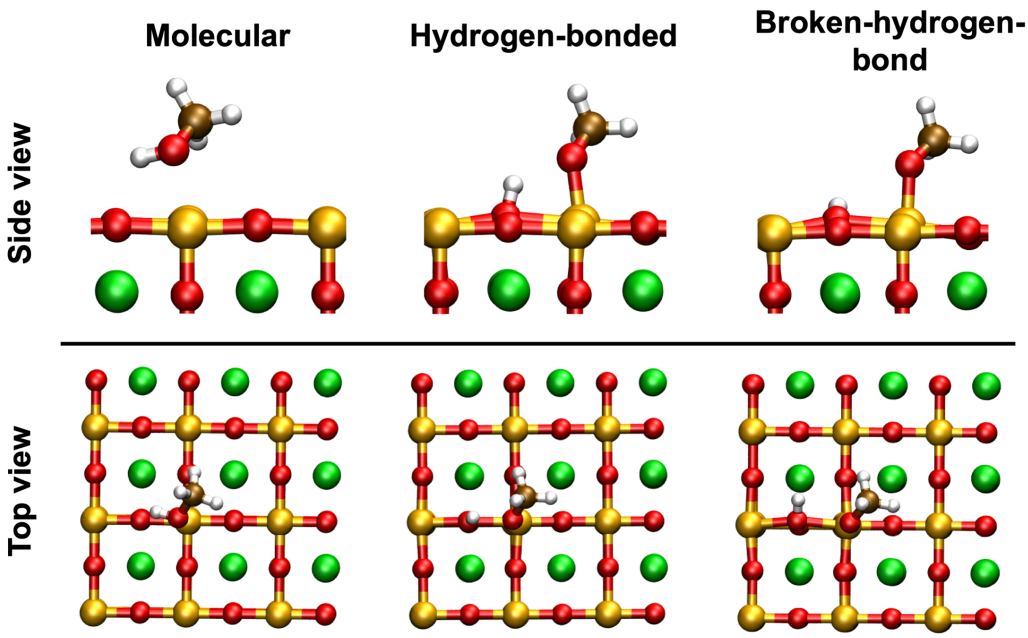

Figure S8: DFT-computed structures of methanol/STO(100) in the minimum-energy orientation presented in Figure 4 of the main text.

Table S9: DFT-computed adsorption energies, O-H stretching frequencies, and selected geometric features of methanol/STO(100) presented in Figure 4 of the main text.

Methanol	Molecular	Deprotonated, Hydrogen-bonded	Deprotonated, broken-hydrogen-bond
E_{ads}, eV	**1.10**	**1.26**	**1.37**
p, 298 K	0.00%	3.98%	96.02%
O_{alk}-H_{alk} stretching frequency, cm^{-1}	3437		
O_{surf}-H_{alk} stretching frequency, cm^{-1}		3383	3580
Ti-O_{alk}	2.21 Å	1.96 Å	1.92 Å
O_{alk}-H_{hyd}	0.99 Å	1.91 Å	2.77 Å
O_{surf}-H_{hyd}	2.05 Å	0.99 Å	0.98 Å
O_{alk}-Ti-O_{surf}	77.3°	77.8°	87.7°
H_{hyd}-O_{surf}-(0,0,1)	102.2°	16.0°	64.6°
H_{hyd}-O_{surf}-Ti	89.3°	82.0°	94.4°

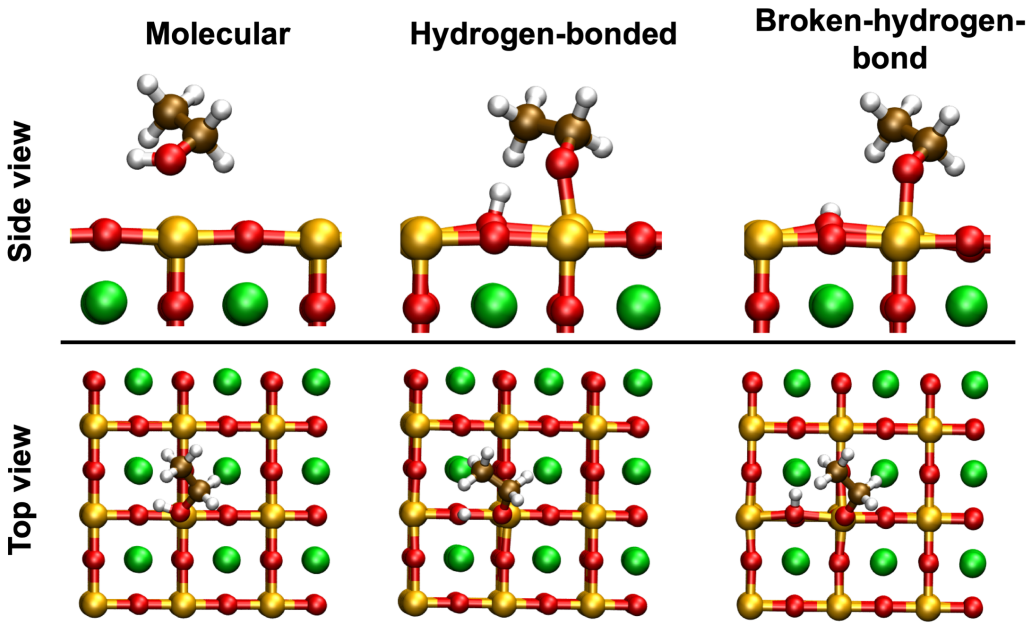

Figure S9: DFT-computed structures of ethanol/ STO(100) in the minimum-energy orientation presented in Figure 4 of the main text.

Table S10: DFT-computed adsorption energies, O-H stretching frequencies, and selected geometric features of ethanol/STO(100) presented in Figure 4 of the main text.

Ethanol	Molecular	Deprotonated, Hydrogen-bonded	Deprotonated, broken-hydrogen-bond
E_{ads}, eV	1.17	1.37	1.43
p, 298 K	0.00%	9.30%	90.70%
-OH stretching frequency, cm^{-1}	3608	3331	3586
Ti-O_{alk}	2.20 Å	1.96 Å	1.92 Å
O_{alk}-H_{hyd}	0.98 Å	1.88 Å	2.75 Å
O_{surf}-H_{hyd}	2.37 Å	0.99 Å	0.98 Å
O_{alk}-Ti-O_{surf}	83.3°	77.5°	87.5°
H_{hyd}-O_{surf}-(0,0,1)	89.7°	13.3°	63.2°
H_{hyd}-O_{surf}-Ti	96.8°	80.6°	94.4°

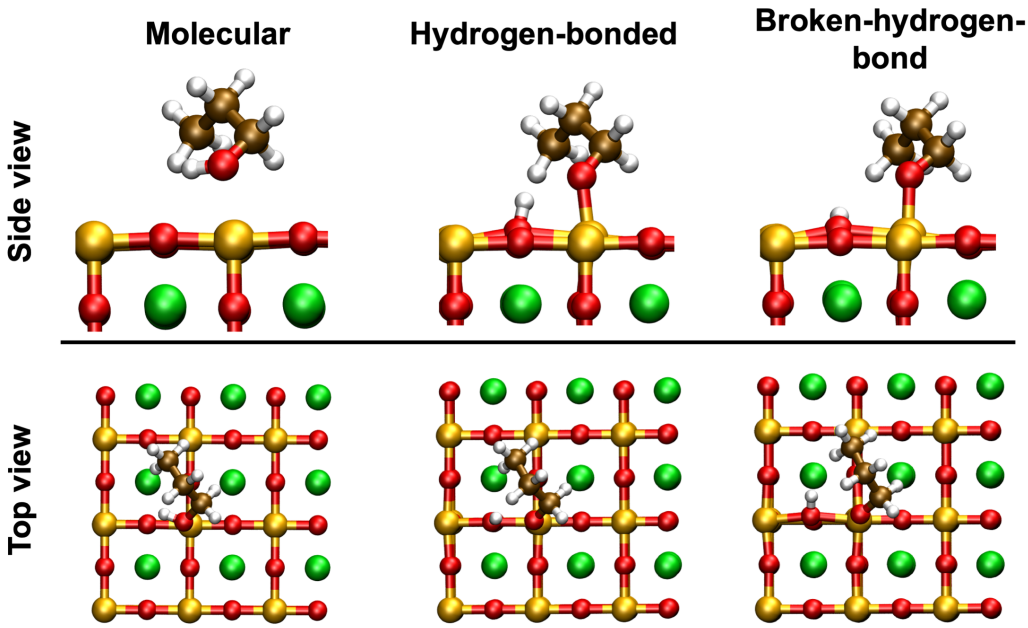

Figure S10: DFT-computed structures of n-propanol/STO(100) in the minimum-energy orientation presented in Figure 4 of the main text.

Table S11: DFT-computed adsorption energies, O-H stretching frequencies, and selected geometric features of n-propanol/STO(100) presented in Figure 4 of the main text.

N-propanol	Molecular	Deprotonated, Hydrogen-bonded	Deprotonated, broken-hydrogen-bonded
E_{ads}, eV	1.26	1.47	1.58
p, 298 K	0.00%	1.65%	98.35%
-OH stretching frequency, cm^{-1}	3551	3422	3593
Ti-O_{alk}	2.20 Å	1.96 Å	1.93 Å
O_{alk}-H_{hyd}	0.98 Å	1.93 Å	2.69 Å
O_{surf}-H_{hyd}	2.24 Å	0.99 Å	0.98 Å
O_{alk}-Ti-O_{surf}	80.4°	77.9°	86.2°
H_{hyd}-O_{surf}-(0,0,1)	95.6°	15.8°	64.1°
H_{hyd}-O_{surf}-Ti	93.7°	83.4°	94.9°

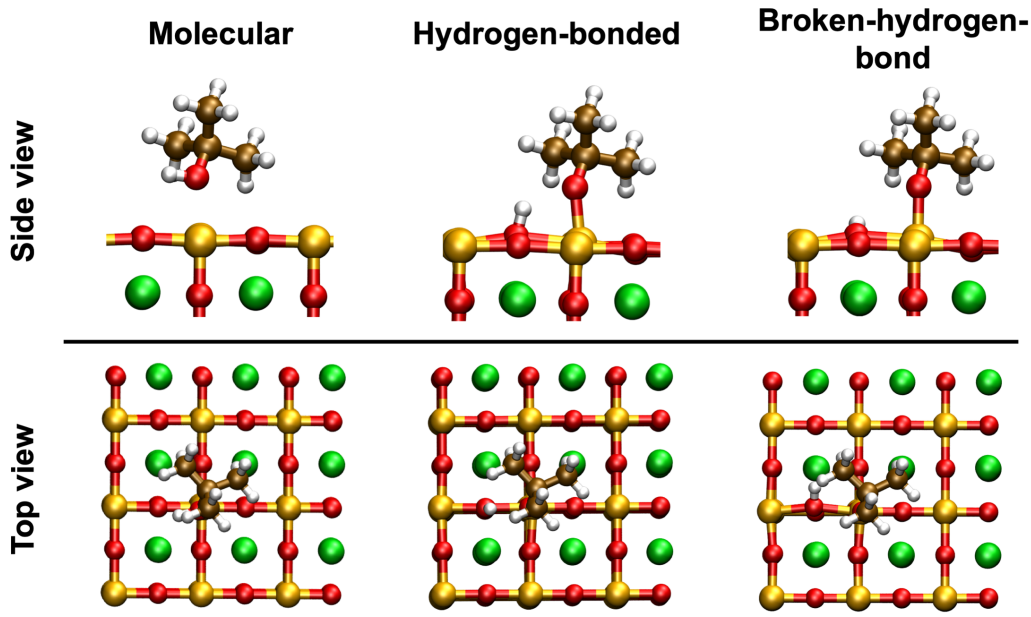

Figure S11: DFT-computed structures of tert-butanol/STO(100) in the minimum-energy orientation presented in Figure 4 of the main text.

Table S12: DFT-computed adsorption energies, O-H stretching frequencies, and selected geometric features of tert-butanol/STO(100) presented in Figure 4 of the main text.

Tert-butanol	Molecular	Deprotonated, Hydrogen-bonded	Deprotonated, broken-hydrogen-bonded
E_{ads}, eV	1.29	1.43	1.48
p, 298 K	0.07%	13.13%	86.81%
-OH stretching frequency, cm^{-1}	3628	3409	3582
Ti-O_{alk}	2.21 Å	1.95 Å	1.91 Å
O_{alk}-H_{hyd}	0.98 Å	1.95 Å	2.80 Å
O_{surf}-H_{hyd}	2.47 Å	0.99 Å	0.98 Å
O_{alk}-Ti-O_{surf}	84.7°	78.8°	87.0°
H_{hyd}-O_{surf}-(0,0,1)	84.5°	13.3°	64.6°
H_{hyd}-O_{surf}-Ti	100.3°	82.3°	94.9°

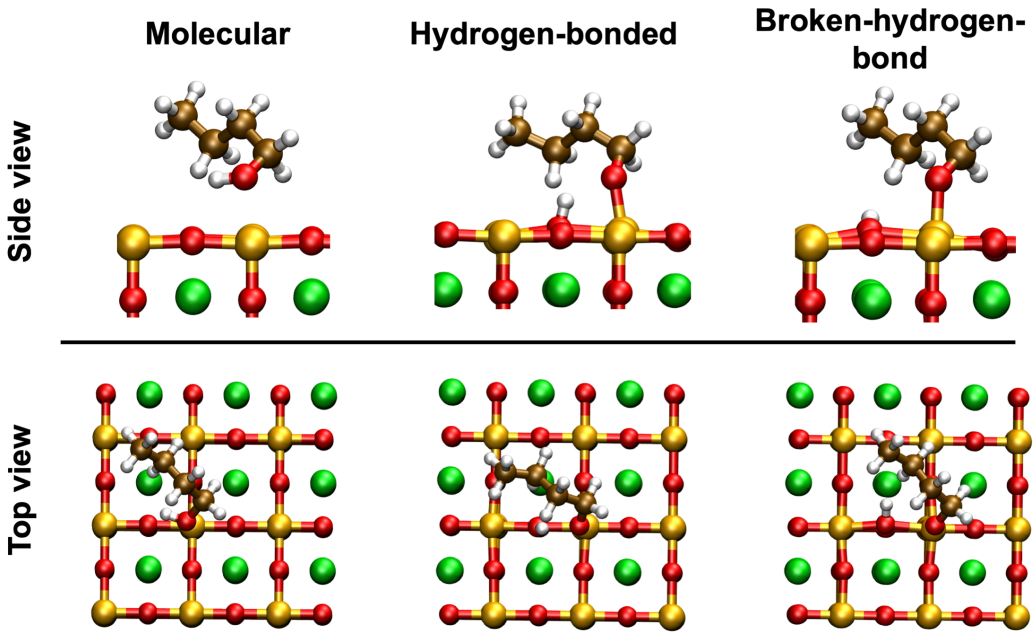

Figure S12: DFT-computed structures of n-butanol/STO(100) in the minimum-energy orientation presented in Figure 4 of the main text.

Table S13: DFT-computed adsorption energies, O-H stretching frequencies, and selected geometric features of n-butanol/STO(100) presented in Figure 4 of the main text.

N-butanol	Molecular	Deprotonated, Hydrogen-bonded	Deprotonated, broken-hydrogen-bonded
E_{ads}, eV	1.34	1.48	1.60
p, 298 K	0.00%	1.05%	98.94%
-OH stretching frequency, cm^{-1}	3532	3348	3580
Ti-O_{alk}	2.20 Å	1.96 Å	1.92 Å
O_{alk}-H_{hyd}	0.98 Å	1.89 Å	2.75 Å
O_{surf}-H_{hyd}	2.27 Å	0.99 Å	0.98 Å
O_{alk}-Ti-O_{surf}	80.9°	77.5°	87.0°
H_{hyd}-O_{surf}-(0,0,1)	94.1°	13.7°	64.5°
H_{hyd}-O_{surf}-Ti	94.4°	80.5°	94.7°

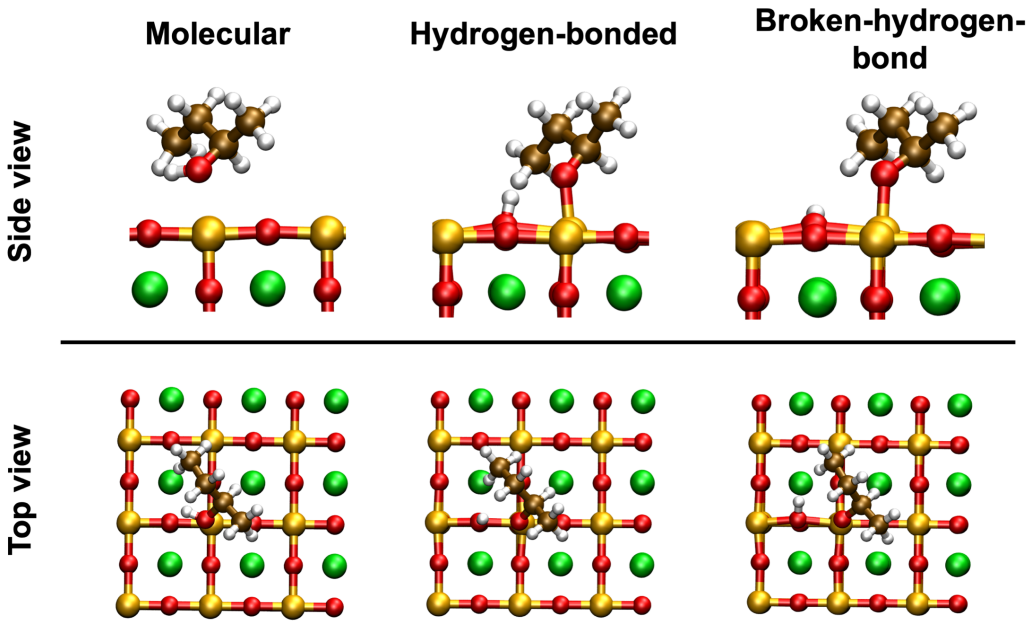

Figure S13: DFT-computed structures of sec-butanol/STO(100) in the minimum-energy orientation presented in Figure 4 of the main text.

Table S14: DFT-computed adsorption energies, O-H stretching frequencies, and selected geometric features of sec-butanol/STO(100) presented in Figure 4 of the main text.

Sec-butanol	Molecular	Deprotonated, Hydrogen-bonded	Deprotonated, broken-hydrogen-bonded
E_{ads}, eV	1.35	1.54	1.64
p, 298 K	0.00%	1.63%	98.37%
-OH stretching frequency, cm^{-1}	3571	3440	3592
Ti-O_{alk}	2.20 Å	1.96 Å	1.93 Å
O_{alk}-H_{hyd}	0.98 Å	1.95 Å	2.71 Å
O_{surf}-H_{hyd}	2.27 Å	0.99 Å	0.98 Å
O_{alk}-Ti-O_{surf}	80.5°	77.9°	86.4°
H_{hyd}-O_{surf}-(0,0,1)	95.0°	19.5°	64.4°
H_{hyd}-O_{surf}-Ti	94.6°	84.2°	95.0°

I.G. Interactions between alkyl groups and the surface

The interaction between the alkyl groups in adsorbed alkanols and the surface is dominated by van der Waals interactions, which, in this work have been included by applying the Grimme's D3 dispersion correction in our geometry optimizations using DFT. Thus, to evaluate the role of alkyl-surface interactions on interfacial acidity, differences in energy between the two deprotonated chemisorption states can be compared in calculations that either include or omit this D3 dispersion correction from geometry optimizations. Table S15 gives the DFT energies of the hydrogen-bonded and broken-hydrogen-bond states for ethanol, isopropanol, and n-butanol, as well as the difference in energy, ΔE between these two states for each alkanol. The first column in the table reports the DFT results corresponding to the K_{ia} values in Figure 4 of the main text; that is, these structures have been optimized with dispersion. The second column reports energies for the same alkanols that have been optimized without dispersion. The final column provides the difference between ΔE values obtained as a result of including or omitting the D3 correction during optimization. Increasing chain length from ethanol to n-butanol results in a threefold increase in ΔE due to the dispersion correction, suggesting a greater role of alkyl-surface interactions in the longer alkanol than in the shorter one. Conversely, increasing substitution from ethanol to isopropanol does not significantly change ΔE due to dispersion, implicating alkyl-surface interactions to a similar extent in both of these alkanols.

Table S15: DFT energies (eV) for structures optimized both with and without Grimme's D3 dispersion correction

	dispersion	no dispersion	difference
ethanol			
h-bonded	-1128.964162	-1107.390939	
broken h-bond	-1129.022659	-1107.440716	
ΔE	-0.05849699	-0.0497772	**0.00871979**
isopropanol			
h-bonded	-1145.700943	-1124.037346	
broken h-bond	-1145.737517	-1124.066798	
ΔE	-0.0365742	-0.02945152	**0.00712268**
n-butanol			
h-bonded	-1162.196849	-1140.399038	
broken h-bond	-1162.313504	-1140.487773	
ΔE	-0.11665449	-0.08873503	**0.02791946**

I.H. Interfacial acidity

The interfacial acid dissociation constant, K_{ia}, of the adsorbed alkanol is defined as

$$K_{ia} = \frac{[RO^-]_{ads}[H^+]_{ads}}{[RO^{\delta-} \cdots H^{\delta+}]_{ads}} = \frac{(Q_{vib}Q_{elec})_{[RO^-]_{ads}[H^+]_{ads}}}{(Q_{vib}Q_{elec})_{[RO^{\delta-} \cdots H^{\delta+}]_{ads}}},$$

where Q_{vib} is the canonical vibrational partition function and Q_{elec} is the canonical electronic partition function. In the equation above, numerators correspond to broken-hydrogen-bond species (i.e., "products" in Table S16), and denominators to hydrogen-bonded species ("reactants"). The partition functions were calculated using the expressions

$$Q_{elec} = e^{-\frac{E_{elec}}{k_B T}} = e^{-\frac{E_{ads}}{k_B T}} \text{ and}$$

$$Q_{vib} = \prod_{i=1}^{n} \frac{e^{-\frac{h\nu_i}{2k_B T}}}{1 - e^{-\frac{h\nu_i}{k_B T}}},$$

where E_{elec} = electronic energy, E_{ads} = adsorption energy, ν_i = i-th normal-mode frequency, n = number of normal modes, T = temperature, h = Planck's constant, and k_B = Boltzmann constant.[2, 3]

The electronic energies and vibrational frequencies used to calculate partition functions were computed using DFT. Frequencies were calculated from optimized geometries using density functional perturbation theory without applying symmetry. For normal-mode calculations, all atoms were frozen except those in the alkanol adsorbate (including the acidic proton) and the Ti and O_{surf} atoms to which O_{alk} and H_{hyd} bond in dissociative chemisorption. Only real frequencies were found in the normal-mode calculations for all minima.

Table S16: Partition functions, K_{ia}, and pK_{ia} of adsorbed alcohols on STO(100) at 298K

Alcohol	$\frac{(Q_{elec})_{products}}{(Q_{elec})_{reactants}}$	$\frac{(Q_{vib})_{products}}{(Q_{vib})_{reactants}}$	K_{ia}	pK_{ia}
Methanol	24.11	0.94	22.66	-1.36
Ethanol	9.75	0.74	7.24	-0.86
n-propanol	59.40	0.42	24.96	-1.40
iso-propanol	36.86	0.38	14.11	-1.15
n-butanol	93.73	0.66	61.69	-1.79
sec-butanol	60.39	0.36	21.98	-1.34
tert-butanol	6.61	0.50	3.32	-0.52

At T=500K, the trends for acidity with respect to chain length and α-carbon substitution are similar to those at 298K. As such, as temperature increases, the role of chain length (as compared to that of substitution) in interfacial acidity increases as well. pK_{ia} values at 500K are provided in Table S17 and plots of pK_{ia} values at 500K as functions of x and y are provided in Figure S14.

Table S17: Partition functions, K_{ia}, and pK_{ia} of adsorbed alcohols on STO(100) at 500K

Alcohol	$\frac{(Q_{elec})_{products}}{(Q_{elec})_{reactants}}$	$\frac{(Q_{vib})_{products}}{(Q_{vib})_{reactants}}$	K_{ia}	pK_{ia}
Methanol	6.67	1.02	6.78	-0.83
Ethanol	3.89	0.83	3.23	-0.51
n-propanol	11.42	0.48	5.53	-0.74
iso-propanol	8.59	0.44	3.81	-1.02
n-butanol	14.99	0.69	10.38	-0.21
sec-butanol	11.53	0.43	4.94	-0.69
tert-butanol	3.08	0.56	1.78	-0.25

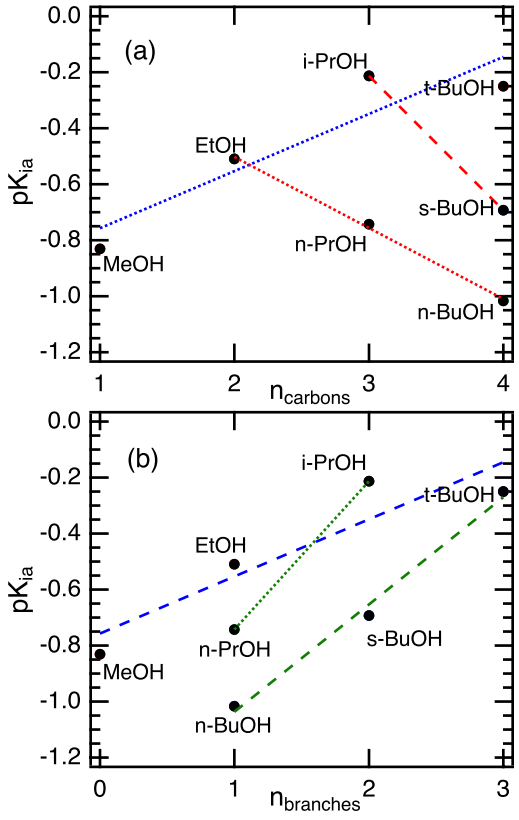

Figure S14: pK_{ia} values for alkanols from methanol to butanol adsorbed on STO(100) at 500 K. DFT-computed values (black circles) are shown as a function of the total number of carbon atoms ($n_{carbons}$) in (a) and as a function of alkyl substituents on the α carbon

($n_{branches}$) in (b). The linear-fit equations in (a) are, $pK_{ia} = -0.96 + 0.20n_{carbons}$ (dotted blue, $R^2 = 0.85$), $pK_{ia} = -0.25n_{carbons}$ (dotted red, $R^2 = 1.00$), and $pK_{ia} = 1.23 - 0.48n_{carbons}$ (dashed red, $R^2 = 1$), and in (b) are, $pK_{ia} = -0.76 + 0.20n_{branches}$ (dashed blue, $R^2 = 0.85$), $pK_{ia} = -1.27 + 0.53n_{branches}$ (dotted green, $R^2 = 1$), and $pK_{ia} = -1.42 + 0.38n_{branches}$ (dashed green, $R^2 = 0.99$).

II. Experimental Results

II.A. X-Ray diffraction

We collected x-ray diffraction patterns of the single crystal (001) STO sample (obtained from MTI Corp.) before and after SFG experiments using a Scintag PDS 2000 diffractometer equipped with Cu-K_α radiation and a nickel filter. Scattering angles of 20–80° were collected in 0.02° steps with a count time of 1 s per step. Z-alignment errors are not corrected for. Phase identification was performed using PANalytical HighScore Plus software package and indexing to diffraction files (COD, 96-900-6865). Figure S13 shows that the sample is single crystalline as only the (002) reflection is clearly observed. The (001) and (003) reflections are naturally weak for STO. After the experiment, there is no change in the diffraction pattern, indicating no restructuring due to alkanol adsorption at room temperature.

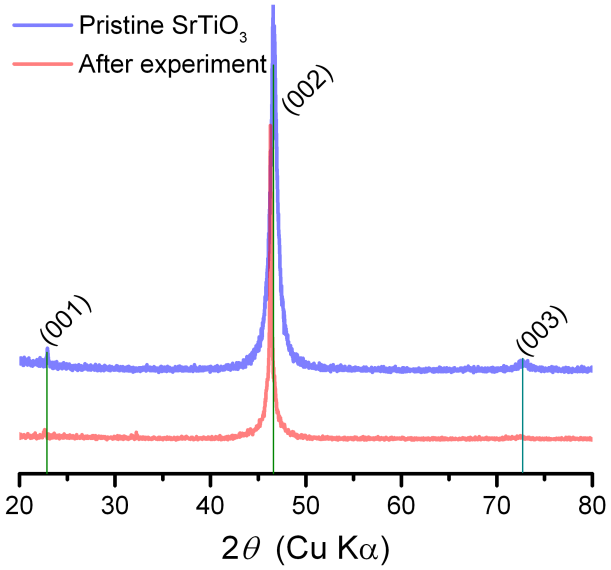

Figure S15. XRD of STO single crystal sample before and after experiment. Lines mark (00*l*) reflections.

II.B. Atomic force microscopy

STO Atomic force micrographs, shown in Figure S14, were conducted on a WITec Alpha 300 in contact mode atop an active vibration cancelation pad. Micrographs are composed of 265 x 265 pixels for a total area of either 25 μm^2 or 0.25 μm^2. Each line scan took 2 s round trip and drift was corrected using a smooth background and a 3x3 pixel average was applied. Surface roughness was found to be ~0.5 nm RMS.

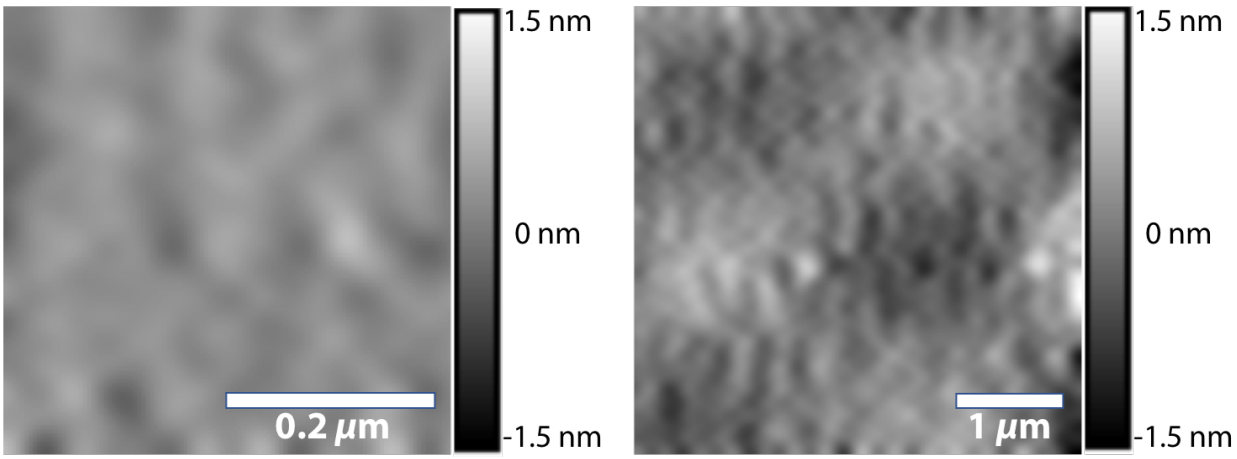

Figure S16. ARM images of pristine STO sample at two magnifications.

III. References

1. Sholl, D.; Steckel, J. A., *Density functional theory: a practical introduction*. John Wiley & Sons: 2011.
2. McQuarrie, D., *Statistical Mechanics*. 2000, Sausalito. California: University Science Books.
3. Hill, T. L., *An introduction to statistical thermodynamics*. Courier Corporation: 1986.